Biosensors and Bioelectronics 226 (2023) 115114

Contents lists available at ScienceDirect

Biosensors and Bioelectronics

journal homepage: www.elsevier.com/locate/bios

Integration of on-chip lysis and paper-based sensor for rapid detection of viral and exosomal RNAs

Jingjing Qian [a], Qinming Zhang [a], Meng Lu [a,b,*]

[a] Department of Electrical and Computer Engineering, Iowa State University, Ames, IA 50011, USA
[b] Department of Mechanical Engineering, Iowa State University, Ames, IA 50011, USA

ARTICLE INFO

Keywords:
Paper-based sensor
Nucleic acid amplification testing (NAAT)
Isothermal amplification
Point-of-care testing (POCT)

ABSTRACT

In recent years, paper-based nucleic acid sensors have been demonstrated for the ability to detect DNA and RNA molecules extracted from viruses and bacteria. In clinical samples, these nucleic acids are mostly encapsulated in lipid membranes and need to be released before being analyzed using paper-based sensors. For the nucleic acid amplification tests (NAATs), it is also desirable to remove the interfering molecules that can inhibit the nucleic acid amplification. To achieve a field deployable NAAT, we report a portable sensor system that combines the thermolysis and paper-based NAATs to detect target RNA molecules carried by viral and exosomal nanoparticles. The sensor cartridge includes a lysis chamber with a pressure-controlled diaphragm valve, paper flow channels, and three paper-based NAAT reaction chambers to extract, transport, and detect nucleic acids respectively. A compact instrument was prototyped to automate the assay, collect fluorescence images of the nucleic acid amplification, and generate amplification curves for NAATs. The pump-free and paper-based sensor achieved quantitative analysis of influenza A virus (IAV) RNA and exosome microRNA within 1 h, with the lowest detect concentration of 10^4 $TCID_{50}$/mL and 10^6 EV/mL for IAV and exosome, respectively. Owing to the advantages of easy storage, simple operation, and low cost, such as system has great potential to be used as a point-of-care test for in-field diagnosis of viral and bacterial infections.

1. Introduction

Paper-based sensors are widely used as a point-of-care test (POCT) for disease diagnosis in resource limited settings. Advantages of paper-based POCTs include, but are not limited to, ease of use, low price due to the use of disposable sensors, capability of reagent storage in paper, and integration of sample loading, transportation, and separation step for fast return of test results (Liana, 2012; Noviana et al., 2021; Yamada et al., 2017; Kaur and Bhushan, 2018; Liu et al., 2019, 2020, 2021, 2022; Gao et al., 2020). The later flow assay (LFA) built upon paper strips have been successfully implemented for the detection of a variety of analytes, such as antigens and drug compounds (Posthuma-TrumpieGeertruida and KorfAart van Amerongen, 2009; Parolo et al., 2020; Carrell et al., 2019; Zhao et al., 2016). The best-known application of LFA is the home pregnancy test for human chorionic gonadotropin in urine samples (Nguyen et al., 2020; Lee et al., 2013). More recently, during the COVID-19 pandemic, the quick home tests of COVID infection predominately reply on LFA sensor for detection of SARS-CoV-2 antigens (Hsiao et al., 2021; Roda et al., 2021; Oh et al., 2022; Grant et al., 2020).

In contrast to the micro-total analysis systems enabled by microfluidic technologies with well-designed pumps, mixers, and valves, the paper-based sensors' capability of processing samples is still limited (Cunningham et al., 2016; Mahato et al., 2017). For example, it is challenging to detect nucleic acids carried by micro- and nano-organisms using paper-based sensors, since the nucleic acids are wrapped in lipid membranes. Upstream lysis and nucleic acid extraction processes are required before the paper-based sensor can be implemented to quantify the target DNAs or RNAs. Although some works showed that the lysis step can be combined with the nucleic acid amplification tests (NAATs), such as quantitative polymerase chain reaction (qPCR) or loop-mediated isothermal amplification (LAMP) assays for the detection of SARS-CoV-2 viruses, the inferencing molecules cause large variations in the test results (Vasudevan et al., 2021; Wee, 2020; Thompson and Lei, 2020). It is highly desirable to lyse lipid membranes and release nucleic acids from cells or viruses for quantitative analysis.

Common lysis methods include thermal, chemical, lysozyme, or bead-beating treatments that can disrupt the lipid membranes (Grigorov and KirovMarin, 2021). The chemical and enzymatic treatments are

* Corresponding authorDepartment of Electrical and Computer Engineering, Iowa State University, Ames, IA 50011, USA
E-mail address: menglu@iastate.edu (M. Lu).

https://doi.org/10.1016/j.bios.2023.115114
Received 3 November 2022; Received in revised form 15 January 2023; Accepted 30 January 2023
Available online 1 February 2023

simple but require additional steps to extract nucleic acids and remove the chemicals that interfere with the downstream NAATs (Al-Soud et al., 2001; Svec et al., 2013). The mechanic disruption lysis processes require a homogenizer and are not suitable for POCT applications. In contrast, thermolysis is capable of lysing cells and viral nanoparticles by a simple heating process without introducing potential PCR inhibitors. The use of thermolysis in a paper-based POCT system can significantly simplify the detection of RNAs encapsulated by lipid membranes, enable quantitative analysis, and offer improved repeatability.

This paper reports the integration of pump-free nucleic acid extraction and a paper-based sensor for the detection of RNAs wrapped in lipid nanoparticles, such as viruses and exosomes. The sensor cartridge, as shown in Fig. 1, includes a thermolysis chamber with a pressure-controlled diaphragm valve, a paper fluidic channel, and three paper-based reaction pads, in which the assay reagents are stored. Users only need to load samples into the thermolysis chamber, and an Arduino microchip manages two heaters and acquires fluorescence images to execute the entire assay. During a test, the samples in the thermolysis chamber, were heated to release nucleic acids and evaporated through the nozzle at the center of the diaphragm. The sample vapor is subsequently collected by the paper strip and transferred to the reaction pads for the detection of target nucleic acids. Two isothermal amplification approaches, LAMP and exponential amplification reaction (EXPAR), were implemented for the detection of RNA in influenza A virus (IAV) and microRNA (miRNA) carried by macrophage-derived exosomes (Fig. 1(f) and **(g)**), respectively. The pump-free and paper-based system can extract nucleic acids and quantify their concentrations within 1 h.

2. Experiments and methods

2.1. Materials and reagents

All DNA oligonucleotides were ordered from Integrated DNA Technologies Inc.. The WarmStart LAMP master mix (E1700L), SYBR-green fluorescence dye (B1700S), LAMP reaction buffer (NEBuffer™ 3.1, B7203S), and nicking endonuclease (Nb.BsrDI, R0648S) were purchased from New England Biolabs Inc.. Diethylpyrocarbonate (DEPC)-treated water, Tris-EDTA (TE) buffer, trehalose, and bovine serum albumin (BSA) were obtained from Fisher Scientific. The single strand binding (SSB) protein and filter papers were purchased from Sigma Aldrich Inc. and SteriTech Inc., respectively. The microcontroller (ESP32), CMOS cameras (OV2640), blue LEDs (732-4966-1-ND), and a LED driver (HV9803BLG-GCT-ND) were bought from Digi-Key Electronics. The excitation (FGB25) and emission filters (FGL530) were obtained from Thorlabs Inc..

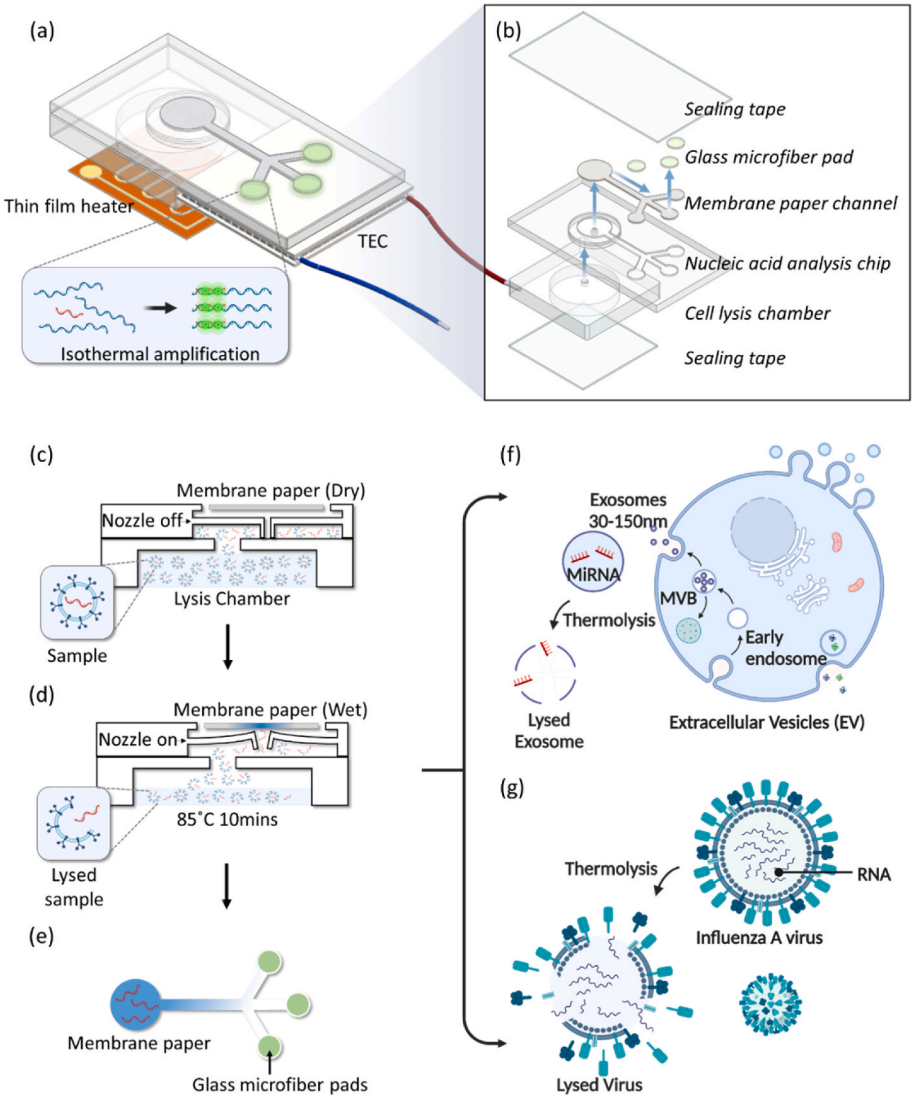

Fig. 1. Schematic diagram of the pump-free sensor chip for nucleic acid extraction and detection. (a) Assembled sensor cartridge attached to a thin-film heater and TEC to for thermolysis and nucleic acid amplification processes, respectively. (b) Exploded view of the sensor cartridge with the paper-based flow channel and NAAT reaction pads. (c) and (d) Cross section of the heat lysis chamber capped by a diaphragm valve. (e) Transportation of lysed sample in the paper flow strip. (f) Schematics of macrophage-derived exosome with the microRNA cargo. (g) Thermolysis of Influenza A virus to release viral RNA.

2.2. Design and fabrication of sensor cartridge

The sensor cartridge consists of a thermal lysis compartment, a channel for lateral sample transport, and three chambers for nucleic acid amplification and detection, as shown in Fig. 1(a) and **(b)**. These three components are connected using a patterned paper strip (Fig. 1(e)). The thermal lysis compartment relies on a diaphragm valve to control the evaporation of samples. As illustrated in Fig. 1(c) and **(d)**, the diaphragm seals the lysis chamber and a micro nozzle perforated at the center of the diaphragm is designed to release vapors when the chamber exceeds a given threshold. During a thermal lysis process, a thin-film heater is used to heat up the lysis chamber, lyse the viruses or exosomes, and evaporate the lysed sample through the nozzle. The vapor that passes through the nozzle is immediately absorbed by the paper strip and transferred towards the reaction chamber. The dimension and material of the diaphragm were carefully chosen and optimized using simulation to achieve the chamber pressure of 10 kPa at 10 min. The thickness and outer diameter of the diaphragm valve are 0.5 mm and 15 mm, respectively. The micro nozzle has a thickness of 1.2 mm and inner diameter of 1 mm. The diameter and depth of the thermolysis chamber are 20 mm and 4 mm, respectively. The paper strip channel has a length of 15 mm and a width of 2 mm. The diameter of the nucleic acid amplification reaction chambers is 5 mm. The disposable sensor cartridges were 3D-printed with a biocompatible nylon by Shapeways Inc.

2.3. Isothermal NAATs and reagents

The exosomal miRNAs and viral RNAs were detected using the exponential isothermal amplification (EXPAR) and LAMP assays, respectively. Both EXPAR and LAMP are well-established miRNA detection assay and their amplification mechanism are summarized in Fig. S1. The EXPAR assay amplify target miRNAs utilizing a single-stranded DNA (ssDNA) template, whose sequence consists of two identical miRNA sequence (Qian et al., 2022). Briefly, the target miRNAs can anneal to the 3' end of the ssDNA template and be extended by a strand-displacing DNA polymerase (Bst2.0) to produce a double-stranded DNA (dsDNA) amplicon. After being restricted by the nicking enzyme at the center, both left and right half of the replica can function as a primer to produce more dsDNA amplicons, which is quantified using a dsDNA binding dye (SYBR-green). Hongxia Jia et al. demonstrated the EXPAR miRNA assay that can distinguish one base difference such as let-7 family miRNAs (Jia et al., 2010). The EXPAR reagent consists of the SSB protein (2 μM), RNase inhibitor (0.8 U/μL), SYBR-green dye (0.4 μg/mL), WarmStart Lamp Master Mix, and nicking endonuclease (0.4U/μL). The ssDNA template sequence for the detection of exosomal miRNA223 is listed in Fig. S2. The ssDNA templates (0.2 μM) and reagents were mixed in the DEPC-treated water. The LAMP assay uses six pairs of primers (Fig. S2) and the same displacement DNA polymerase, to amplify a target sequence (Moranova et al., 2022). The LAMP reagent consists of SYBR-green dye (0.4 μg/mL), LAMP master mix, three pairs of primers. During a LAMP reaction, the reverse transcriptase in the LAMP Master mix can generate complimentary DNA from the viral RNA. The LAMP primer pairs were designed to amplify the hemagglutinin (HA) gene of the influenza A virus (Manmohan Parida 1 et al., 2011; Diaz et al., 2013). Both EXPAR and LAMP reagent compositions were optimized based on our previous work (Liu et al., 2020; Qian et al., 2022).

2.4. Paper-based lateral flow channel and reaction pads

The evaporated sample was condensed and collected using a cellulose paper strip (Fig. 1(c)) placed right above the nozzle. The 100-μm thick cellulose paper was patterned using a cutter to the channel shape as shown in Fig. 1(e). The vapor collection region has a diameter of 12 mm and the diameter of the reaction pads is 5 mm. The glass microfiber filter is chosen as the reaction pad to reduce background fluorescence signal. The reagents required for the isothermal assays were lyophilized in the glass microfiber reaction pads using a freezing dryer. In order reduce non-specific absorption loss of EXPAR or LAMP reagents, the reaction pads were treated using 1 mg/mL BSA for 1 h and dried overnight. To improve the stability of the reagents, 10% of trehalose was added prior to the lyophilization (Kumar, 2020). Each 5-mm reaction pad was loaded with 7 μL reagents and lyophilized at −40 °C for 24 h. Finally, the paper strip and three reaction pads were assembled and sealed in the sensor cartridge. The unused reaction pads containing assay reagents were stored in a vacuum-sealed bag under room temperature ~23 °C. For the test performed during a two-month period, no change was found in the RNA amplification capability. As reported in (Kumar, 2020), the reaction pads should be stable for over a year.

2.5. Preparation of exosome and virus samples

Exosomes used in this study were secreted by murine macrophages (J774.1 cell line, ATCC) and extracted using the conventional ultracentrifuge method (WangWang et al., 2018). In brief, the exosomes were sampled from three macrophage phenotype cultures when macrophage reached 90% confluency. The samples were filtered using a 0.22-μm filter to remove cells and debris and then centrifuged at 120,000×*g* for 90 min. The pellet of exosome was resuspended in PBS and transferred into a 1.5 mL centrifuge tube for another 2 h centrifugation at 186,000×*g* at 4 °C.

The IAV samples were propagated and isolated in MDCK cells (CCL-34, ATCC) following a published protocol (Manmohan Parida 1 et al., 2011). This IAV isolate stock had an infectious concentration of 10^7 median tissue culture infectious dose per mL ($TCID_{50}$/mL). The IAV clinic samples, including oral fluids, nasal swabs, and lung tissue homogenates, were obtained from the Veterinary Diagnostic Laboratory of Iowa State University. The clinic samples were analyzed using the conventional RT-qPCR and paper-based LAMP assays to determine the IAV concentrations. TEM images of exosomes and IAV samples are shown in Fig. S3.

2.6. Compact and portable readout instrument

A compact reader, shown in Fig. 2, was prototyped to control the sample lysis, nucleic acid extraction and detection processes. The sensor cartridge, heaters, and fluorescence detector were installed in a 3D-printed housing. In addition, a fixture (Fig. 2(b)) was also 3D-printed to hold the lysis chamber and sensor cartridge together. The lysis chamber was heated using a 9-W thin-film heater without a temperature control. Because the reaction chambers require more a precise temperature setting, we used a 30 × 30 mm thermoelectric cooler (TEC) and a thermocouple (K-type, Omega Engineering). A proportional–integral–derivative control was implemented to maintain the reactor temperature within ±0.1 °C using an ESP32 microcontroller.

The fluorescence detector, consisting of the blue LED array ($P = 360$ mW), CMOS camera, ESP32 microcontroller and optical filters, was built to measure the SYBR-green emission. The ESP32 microcontroller can turn on and off the LEDs, acquire images from the CMOS camera, and transfer the images to the cloud data storage via a WiFi network. During a test, the fluorescence images were captured every 30s and transmitted to a Google Drive folder and processed using a Python script to generate the amplification curves.

3. Results and discussion

3.1. Heat-driven lysis and transportation of lysate

The thermolysis chamber was designed to release nucleic acids and deliver the lysate to the paper strip, as shown in Fig. 1(c-e). Before being used to detect RNAs, the operation of the diaphragm valve and the sample transportation were studied. The goal is to choose the diaphragm

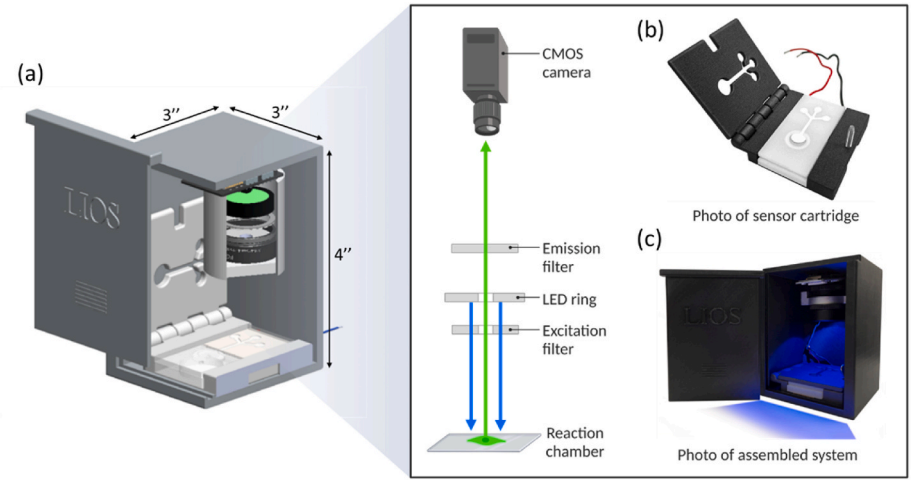

Fig. 2. Portable detection setup enabled by IoT technology. (a) Schematic of the 3D-printed housing for sensor cartridge, heaters, and fluorescence detector. (b) Photo of the sensor cartridge placed inside of a fixture. (c) Photo of the assembled housing with the microcontroller, LED, and camera for fluorescence detection.

geometry that can support chamber temperature and lysis time to achieve a high lysis efficient. In the meantime, the heat generated at the lysis chamber should not affect the assay reagents stored in the reaction chambers. The paper flow channel used to connect the lysis and reaction chambers was designed to ensure sufficient spatial separation, as well as a rapid sample delivery between the chambers.

3.1.1. Simulation of diaphragm valve displacement

To determine the dimension of the diaphragm, the displacements of diaphragm membrane with different geometries were simulated using the finite element method (FEM) simulation (Solid Mechanics Model, COMSOL MultiPhysics). The tensile modulus and tensile strength for the nylon material are 1.6 GPa and 48 MPa, respectively. When the 1-mL lysis chamber is filled with liquid sample and heated to 85 °C, the vapor pressure in the chamber can reach approximately 10 kPa. Fig. 3 (a)-(c) shows the simulated displacement of a nylon diaphragm with the thickness of diameter of 0.5 mm and 15 mm, respectively. A boundary load pressure of 10 kPa was applied from the bottom side of the diaphragm and the other boundaries were fixed. At the center of the diaphragm, the maximum displacement of 0.27 mm along the *y*-axis can be obtained (Fig. 3(b)). It can be seen from the cross-section view in Fig. 3 (a) that this displacement can lift the nozzle and allow the vapor to exit the lysis chamber. Fig. 3(c) compares the simulated displacement as a function of diaphragm thickness from 0.4 to 1 mm. The increase of diaphragm thickness significantly reduces the displacement. On the other hand, a diaphragm thinner than 0.5 mm can open the nozzle too soon even before the sample is fully lysed. To maintain a high lysis efficiency, we designed the diaphragm with a thickness of 0.5 mm.

3.1.2. Temperature distribution around sensor cartridge

The sensor cartridge includes two heating zones for the lysis and the reaction chambers, respectively. To avoid temperature interference, these chambers should be well separated in space. However, a long paper flow channel between these chambers requires excessive time for sample transport. The paper flow channel was designed with a length of 20 mm. To evaluate this design, we measured the temperature distribution in the sensor cassette using a thermal camera (FLIR One Pro) when the lysis and reaction chambers were heated sequentially. Fig. 3(d) shows the measured temperature distributions during different heating steps. While the lysis chamber was heated to 85 °C, the temperature of the reaction chamber can stay at room temperature of 25 °C. During an isothermal amplification, the reaction chambers temperature was stabilized at 58 °C using the TEC and thermistor.

3.1.3. Transportation of evaporated lysate and efficiency of thermolysis

To illustrate the sample lysis and transportation, we filled the lysis chamber with a 1-mL exosome sample dyed with a blue ink (methylene blue). The photos in Fig. 3(e) were taken during sample evaporation and transportation along the 20-mm-long strip. It took up to 10 min for the sample to be evaporated through the nozzle and another 5 min to reach the reaction pads. The flow speed along the paper strip was approximately 10 mm/min. Whenever the reaction pads are fully wicked, the isothermal amplification reaction can start by turning on the TEC heater. To evaluate the lysis efficiency, the solution evaporated through the diaphragm valve was collected and a nanoparticle tracker (Nanosight LM10, Malvern Panalytical) was used to count the number of exosomes. Fig. 4(a) shows the measured size histograms of exosome nanoparticles. The lysis efficiency was calculated by comparing the concentrations of exosomes before and after the 10-min lysis process. The nanoparticles whose diameter is between 50 and 150 nm range were counted. The exosome concentration decreased from 4.4×10^9 EV/mL to 3.0×10^9 EV/mL, which represents a lysis efficiency of approximately 68.2%.

3.2. Extraction of viral RNA for the quantitative detection of IAVs

The swine IAV, which is one of the top agents involved with porcine respiratory disease complex in the US (Salvesen and Whitelaw, 2021; Abhijeet et al., 2021), was chosen as an example to characterize the sensor. Most lab-based tests for swine IAV infections include separated steps of IAV lysis, RNA purification, and reverse transcription-quantitative PCR (RT-qPCR) detection (Manmohan Parida 1 et al., 2011). Here, the RNAs released from swine IAVs were immediately detected using the reverse transcription LAMP (RT-LAMP) assay. The RT-LAMP assay was designed to amplify the hemagglutinin (HA) gene using three set of primers listed in Fig. S2. The RT-LAMP reagents, including the polymerase, primers, SYBR-green dye, were lyophilized in the 5-mm-diameter reaction pads. The compact fluorescence reader can record SYBR-green emission images and determine the RNA concentration based on the time to-threshold value (T_t).

The IVA sample was pipetted into the lysis camber, evaporated through the diaphragm valve for the subsequent RT-LAMP detection. The paper-based RT-LAMP assay was performed at 65 °C and the fluorescence images of the reaction pads were acquired every 30 s. Fig. 4(b) compares the fluorescence images at 0 min, 25 min, 30 min, and 40 min for a 10^8-$TCID_{50}$/mL IAV sample. Two reaction pads contained LAMP primers and the other one was without the primers as the negative control. The increase of SYBR-green emission indicated the production of dsDNA amplicons. The average fluorescence intensity of each reaction

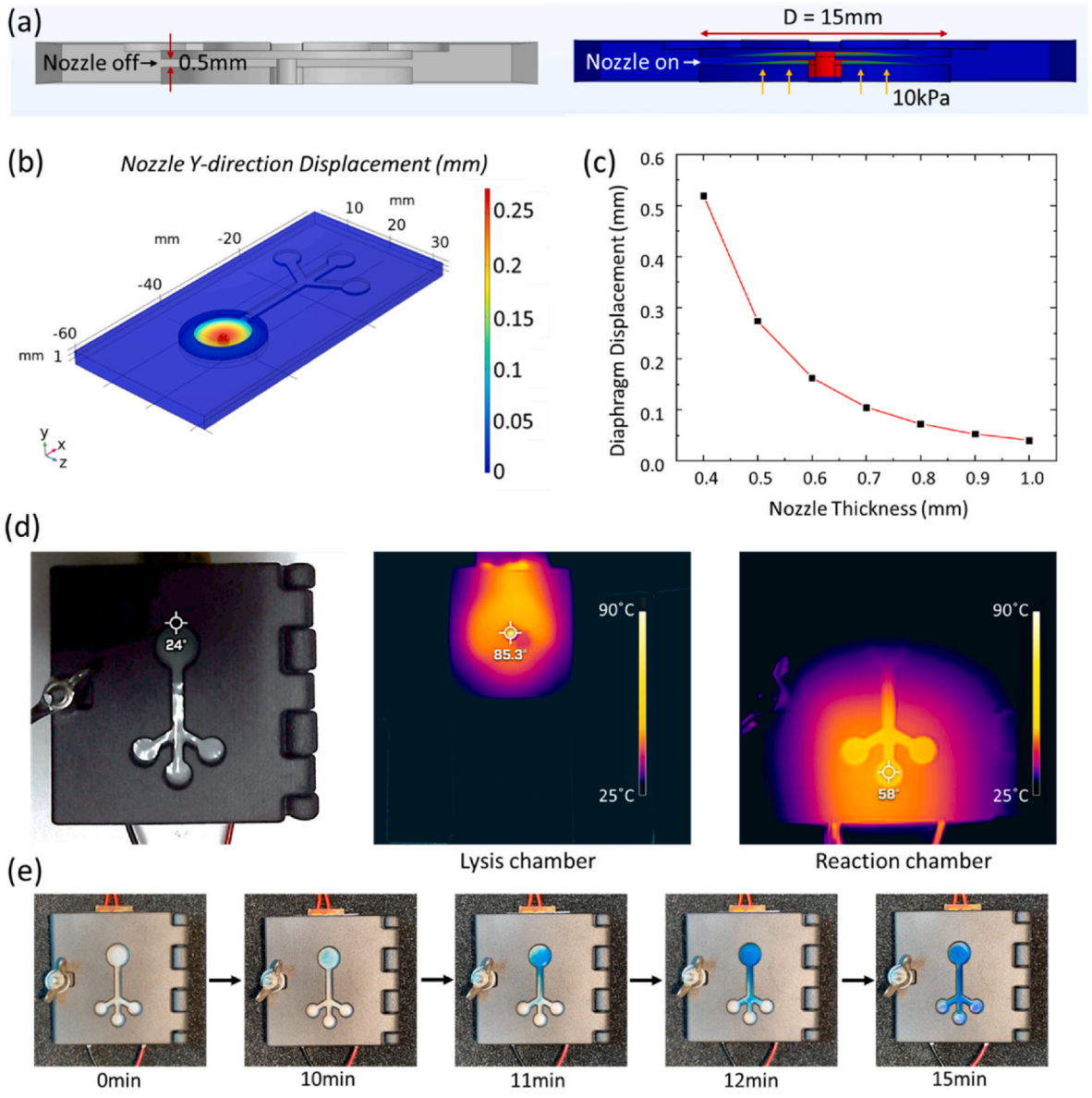

Fig. 3. Heat control diaphragm valve. (a) Cross sectional diagram of the diaphragm with the nozzle (left) and their displacement (right) when the pressure was applied from lysis chamber. (b) Simulated displacement of the diaphragm under a pressure of 10 kPa. (c) Calculated displacement of the diaphragm as a function of the diaphragm thickness. (d) Measured temperature distribution around the sensor cartridge when lysis chamber and reaction chambers were heated to 85 °C and 58 °C, respectively. (e) Images taken during a heat-driven lysis. A blue ink was added to visualize the sample flow.

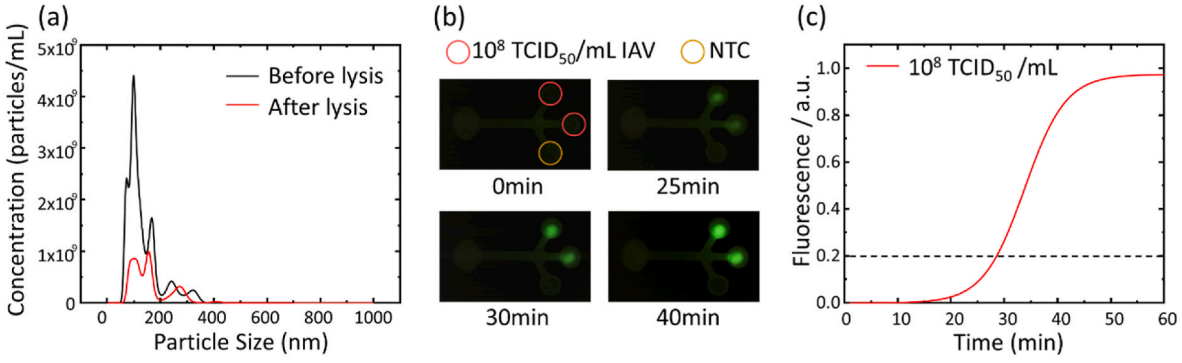

Fig. 4. Lysis of IAV and detection of viral RNA using paper-based LAMP assay. (a) Measured size histograms of exosome sample before and after heat lysis. (b) Fluorescent images of the reaction chambers during a LAMP experiment. (c) Measured the fluorescence intensity as a function of assay time for an IAV sample.

pad was calculated and plotted as a function of time in Fig. 4(c), as the amplification curve. The T_t value, which represents the time when the fluorescence intensity reaches 20% of the maximum fluorescence intensity, was calculated. The T_t value for the 10^8-$TCID_{50}$/mL IAV sample is approximately 29 min.

To characterize the paper-based LAMP assay, a ten-fold dilution series of isolated IAV samples was prepared. The IAV concentration ranged from 10^4 $TCID_{50}$/mL to 10^8 $TCID_{50}$/mL and each sample was tested using one sensor chip. Fig. 5(a) compares the amplification curves measured for these samples. It can be seen from the amplification curves that the amplification started earlier for the sample with a higher IAV concentration. Fig. 5(b) plots the T_t values as a function of IAV concentration from 10^4 to 10^8 $TCID_{50}$/mL. The paper-based LAMP assay can detect IAV with the lowest concentration of 10^4 $TCID_{50}$/mL.

Next, we tested three types of clinic samples, including swine lung homogenate, oral fluid, and nasal swab, collected from pigs. After these clinical samples were filtered using a 0.22 μm filter, each sample was pipetted into the lysis chamber and analyzed using one sensor chip. Fig. 5(c) shows the measured T_t values for lung homogenate, oral fluid, and nasal swab samples, respectively. Clear gaps between positive and negative samples in T_t were found. For the IAV positive samples, the lung homogenate, oral fluid, and nasal swab exhibited averaged T_t value of 23, 34, and 36 min, respectively. The average IAV concentrations in the examined oral fluid, nasal swab, and lung homogenate samples were 6.9×10^{10}, 4.5×10^5, and 5×10^4 $TCID_{50}$/mL. To verify the test results, these clinic samples were also measured using RT-qPCR. The cycle thresholds listed in Fig. S4 agree with the on-chip LAMP result on distinguishing positive and negative samples.

3.3. Extraction of exosomal microRNA for the analysis of exosomes

Protected by lipid membranes, the exosomal miRNAs are more stable than circulating miRNAs, and thus are considered as potential biomarkers for disease diagnosis (Sun et al., 2018). Several miRNA-detection assays have been successfully demonstrated for the detection of exosomal miRNAs (Qian et al., 2022; Ouyang and Liu, 2019; Chen et al., 2011; Jia et al., 2010). Most of these assays requires the lysis of exosomes and extraction of miRNAs. Here, we implemented the paper-based sensor to lyse exosomes and detect the released exosomal miRNAs using the EXPAR assay (Fig. S1(a)). The miRNA-223, which plays a role in regulation of differentiation and phenotype of macrophages, was chosen as an example to characterize the sensitivity of the integrated exosomal miRNA analysis. The exosomes used in study were extracted from murine macrophage culture (WangWang et al., 2018).

A ten-fold dilution of exosomes was prepared with the exosome concentration ranging from 10^6 to 10^{10} EV/mL. The titration of exosomes was thermolyzed and the released miR-223 molecules were measured using the paper-based EXPAR assay. The EXPAR reagents and the ssDNA template (Fig. S2) were lyophilized in the glass microfiber pads. The reaction pads without the ssDNA template served as the non-template control (NTC) reference. When the reaction pads were fully wet, the EXPAR tests were performed at 58 °C for 1 h. For each concentration, the amplification curves were measured and shown in Fig. 6 (a). The miR-223 sample with the highest exosome concentration (10^{10} EV/mL) started to be amplified at a T_t value of 22 min. The NTC sample also showed amplification due to the self-priming effect, but its T_t value was over 63 min. Fig. 6(b) shows the dose-response curve of the exosomal miR-223 by plotting the T_t as a function of exosome concentration. The T_t value decreases with the increase of exosome concentration. When miR-223 is used as a marker for the macrophage-derived exosomes, the sensitivity of this method is approximately 10^6 EV/mL.

4. Conclusion

This work demonstrated the qualitative detection of viral and exsomal RNAs using the integrated thermal lysis and paper-based NAATs. The RNA extraction process ensures the stability and repeatability of the downstream RNA isothermal amplification tests. The pump-free operation and disposable paper-based sensor can reduce the testing cost and simplify the testing process. Meanwhile, the compact readout instrument with the microchip controller offers portable and automatic sample analysis for in-field applications. The sensor chip is capable of measuring IAV and exosome nanoparticles with the sensitivities of as low as 10^4 $TCID_{50}$/mL and 10^6 EV/mL. The results showed that the sensor system can achieve the qualitative detection of viral and exosomal RNAs within 1 h. Compared to POCT sensor based on conventional PCR, the hybrid system significantly reduces the time for cell lysis and DNA purification, as well as the sample collection and transferring time.

Our future work will focus on improving the sensor design from the following aspects. First, the paper-based NAATs can be multiplexed by adding more reaction chambers into the sensor cartridge. The multiplexed detection capability will allow users to detect different types of viruses or multiple microRNAs carried by exosomes. Second, the sensitivity of the assay can be enhanced by optimizing the reagents stored in the reaction pad and reaction conditions. In addition, other nucleic acid tests, such as the Cas9-based RNA detection assays (Olivier et al., 2020), can be adopted with the paper-based sensor. Last but not least, the system will be implemented for rapid identification of bacterial pathogens by lysing bacterial cells, extracting their genomic DNAs or highly conserved 16 S rRNAs, and quantifying the target nucleic acid in the same sensor cartridge.

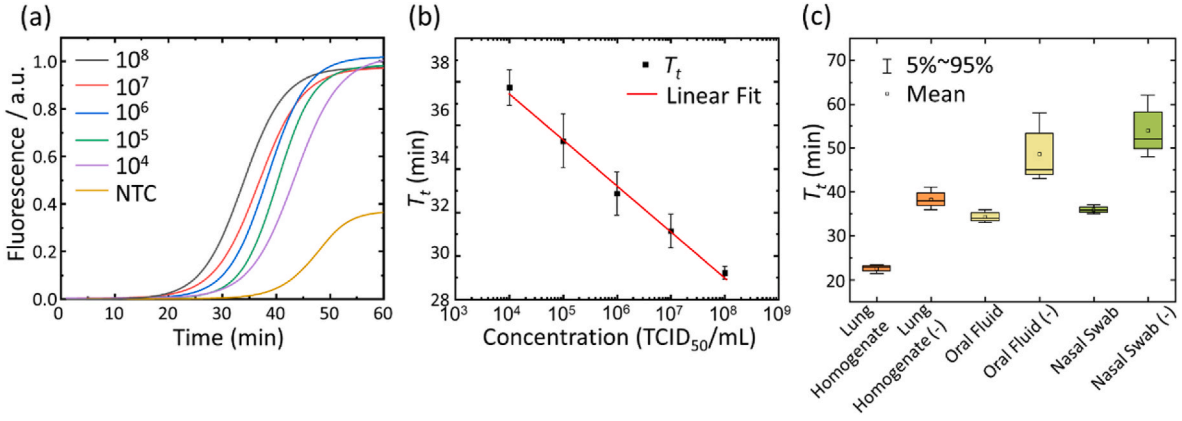

Fig. 5. Paper-based RT-LAMP for quantitative detection of RNAs released from swine IAVs. (a) Amplification curves generated for the LAMP test with a titration of IAV samples ranging from 10^4 to 10^8 $TCID_{50}$/mL. (b) Calculated T_t values *versus* IAV concentration. The error bars represent the standard deviation from three replicated tests. (c) Measured T_t values for homogenate, oral fluid, and nasal swab samples collected from pigs.

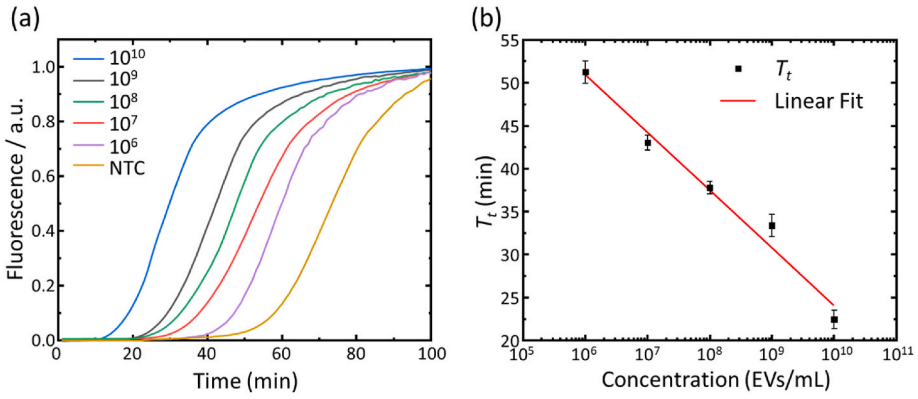

Fig. 6. Quantitative analysis of exosomal miRNA-223 carried by macrophage-derived exosomes. (a) Amplification curves generated for the exosomal wrapped miRNA-223 test with the exosome concentration ranging from 10^6 to 10^{10} EV/mL. (b) Calculated T_t values *versus* exosome concentration. The error bars represent the standard deviation of three repeated measurements.

Credit author statement

Jingjing Qian: Conceptualization, Investigation, Methodology, Validation, Writing – original draft, Writing – review & editing. Qinming Zhang: Investigation, Resources, Methodology. Meng Lu: Conceptualization, Methodology, Writing – original draft, Writing – review & editing.

Declaration of competing interest

The authors declare that they have no known competing financial interests or personal relationships that could have appeared to influence the work reported in this paper.

Data availability

Data will be made available on request.

Acknowledgement

This research was supported by the National Science Foundation under grant ECCS 16-53673. Any opinions, findings, and conclusions or recommendations expressed in this material are those of the author(s) and do not necessarily reflect the views of the National Science Foundation. The authors would thank Prof. Michael Kimber of Iowa State University for providing the macrophages, and Prof. Jiangqiang Zhang for providing the IAV samples.

Appendix A. Supplementary data

Supplementary data to this article can be found online at https://doi.org/10.1016/j.bios.2023.115114.

References

Abhijeet A. Bakre, Les P. Jones, Jackelyn Murray, Z. Beau Reneer, Victoria A. Meliopoulos, Sean cherry, stacey schultz-cherry and ralph A. Tripp, 2021. J. Virol.. 95, 15.
Al-Soud, Abu, Waleed, Rådström, Peter, 2001. J. Clin. Microbiol. 39 (2), 485–493.
Carrell, Cody, Kava, Alyssa, Nguyen, Michael, Menger, Ruth, Munshi, Zarina, 2019. Zachary call, mark nussbaum, and charles henry. Microelectron. Eng. 206, 45–54.
Chen, Caifu, Tan, Ruoying, Wong, Linda, Fekete, Richard, Halsey, Jason, 2011. Methods Mol. Biol. 687, 113–134.
Cunningham, Josephine C., DeGregory, Paul R., Crooks, Richard M., 2016. Annu. Rev. Anal. Chem. 9, 183–202.
Diaz, Andres, Allerson, Matthew, Culhane, Marie, Sreevatsan, Srinand, Torremorell, Montserrat, 2013. Influenza and Other Respiratory Viruses, pp. 52–60, 7 Suppl 4.
Gao, Xin, Li, Xiuyuan, Sun, Xinzhi, Zhang, Jingyan, Zhao, Yuecan, Liu, Xiaojuan, Li, Feng, 2020. Anal. Chem. 92 (6), 4592–4599.
Grant, Benjamin D., Anderson, Caitlin E., Williford, John R., Alonzo, Luis F., Glukhova, Veronika A., Boyle, David S., Weigl, Bernhard H., Nichols, Kevin P., 2020. Anal. Chem. 92 (16), 11305–11309.
Grigorov, Emil, Boris Kirov, Marin B. Marinov, and vassil galabov, 2021. Micromachines. 12, no. 5, 498.
Hsiao, Wesley Wei-Wen, Trong-Nghia, Le, Pham, Dinh Minh, Ko, Hui-Hsin, Chang, Huan-Cheng, Lee, Cheng-Chung, Sharma, Neha, Lee, Cheng-Kang, Chiang, Wei-Hung, 2021. Biosensors 11 (9), 295.
Jia, Hongxia, Li, Zhengping, Liu, Chenghui, Cheng, Yongqiang, 2010. Angew. Chem. Int. Ed. 29, 5498–5501.
Kaur, Navjot, Bhushan, J., 2018. Toley. Analyst 143 (10), 2213–2234.
Kumar, S., 2020. Analyst 145, 6875–6886.
Lee, Linda G., Nordman, Eric S., Johnson, Martin D., Oldham, Mark F., 2013. Biosensors 3 (4), 360–373.
Liana, Devi D., 2012. Burkhard raguse, J. Justin gooding, and edith chow. Sensors 12 (9), 11505–11526.
Liu, Xiaojuan, Li, Xiuyuan, Gao, Xin, Ge, Lei, Sun, Xinzhi, Li, Feng, 2019. ACS Appl. Mater. Interfaces 11 (17), 15381–15388.
Liu, Mingdian, Zhao, Yuxin, Monshat, Hosein, Tang, Zheyuan, Wu, Zuowei, Zhang, Qijing, Lu, Meng, 2020. Biosens. Bioelectron. 169, 112651.
Liu, Xiaojuan, Gao, Xin, Yang, Limin, Zhao, Yuecan, Li, Feng, 2021. Anal. Chem. 93 (34), 11792–11799.
Liu, Xiaojuan, Cheng, Hao, Zhao, Yuecan, Wang, Yue, Li, Feng, 2022. Biosens. Bioelectron. 199, 113906.
Mahato, Kuldeep, Srivastava, Ananya, Chandra, Pranjal, 2017. Biosens. Bioelectron. 96, 246–259.
Manmohan Parida 1, Shukla, Jyoti, Sharma, Shashi, Ranghia Santhosh, Sanna, Ravi, Vasanthapuram, Mani, Reeta, Thomas, Maria, Khare, Shashi, Rai, Arvind, Kant Ratho, Radha, Pujari, Sujit, Mishra, Bijayanti, , Putcha Venkata Lakshmana Rao, Vijayaraghavan, Rajagopalan, 2011. J. Mol. Diagn.: J. Mod. Dynam. 13 (1), 100–107.
Moranova, Ludmila, Stanik, Michal, Roman, Hrstka, Campuzano, Susana, Bartosik, Martin, 2022. Talanta 238, 123064.
Nguyen, Van-Thuan, Song, Seungri, Park, Seungkyung, Joo, Chulmin, 2020. Biosens. Bioelectron. 152, 112015.
Noviana, Eka, Ozer, Tugba, Carrell, Cody S., Link, Jeremy S., McMahon, Catherine, Jang, Ilhoon, Henry, Charles S., 2021. Chem. Rev. 121 (19), 11835–11885.
Oh, Hyun-Kyung, Kim, Kihyeun, Park, Jinhee, Hyungsoon, Im, Maher, Simon, Kim, Min-Gon, 2022. Biosens. Bioelectron. 205, 114094.
Olivier de Jong, G., Murphy, Daniel E., Mäger, Imre, Willms, Eduard, Garcia-Guerra, Antonio, Jerney, J., Gitz-Francois, Lefferts, Juliet, Gupta, Dhanu, Steenbeek, Sander C., van Rheenen, Jacco, El Andaloussi, Samir, Schiffelers, Raymond M., Matthew, J., Wood, A., Vader, Pieter, 2020. Nat. Commun. 11, 1113.
Ouyang, Tinglan, Liu, Zhiyu, 2019. Zhiyi han and qinyu Ge. Anal. Chem. 91, 3179–3186.
Parolo, Claudio, Sena-Torralba, Amadeo, Francisco Bergua, José, Calucho, Enric, Fuentes-Chust, Celia, Hu, Liming, Rivas, Lourdes, et al., 2020. Nat. Protoc. 15 (12), 3788–3816.
Posthuma-Trumpie, Geertruida, A., Korf, Jakob, Aart van Amerongen, 2009. Anal. Bioanal. Chem. 393 (2), 569–582.
Qian, Jingjing, Zhang, Qinming, Liu, Mingdian, Wang, Yixuan, Lu, Meng, 2022. Biosensors and Bioelectronics, vol. 196.
Roda, Aldo, Cavalera, Simone, Di Nardo, Fabio, Calabria, Donato, Rosati, Sergio, Patrizia Simoni, Colitti, Barbara, Baggiani, Claudio, Roda, Matilde, Anfossi, Laura, 2021. Biosens. Bioelectron. 172, 112765.
Salvesen, H.A., Whitelaw, C.B.A., 2021. Porc Health Manag, vol. 7.
Sun, Zhenqiang, Shi, Ke, Yang, Shuaixi, Liu, Jinbo, Zhou, Quanbo, Wang, Guixian, Song, Junmin, Li, Zhen, Zhang, Zhiyong, Yuan, Weitang, 2018. Molecular Cancer, vol. 17.
Svec, David, Andersson, Daniel, Pekny, Milos, Robert Sjöback, Kubista, Mikael, Anders, Ståhlberg, 2013. Front. Oncol. 3, 274.

Thompson, Dorian, Lei, Yu, 2020. Sens Actuators Rep 2 (1), 100017.
Vasudevan, Harish N., Xu, Peng, Servellita, Venice, Miller, Steve, Liu, Leqian, Allan, Gopez, Chiu, Charles Y., Abate, Adam R., 2021. Sci. Rep. 11 (1), 1–9.
Wang, Yifei, Wang, Yuan, Kimber, Michael, Lu, Meng, Dong, Liang, 2018. ACS Sens. 3, 1616–1621.
Wee, Soon Keong, 2020. Suppiah paramalingam sivalingam, and eric peng huat yap. Genes 11 (6), 664.
Yamada, Kentaro, Shibata, Hiroyuki, Suzuki, Koji, Citterio, Daniel, 2017. Lab Chip 17 (7), 1206–1249.
Zhao, Yunfei, Huang, Yin, Zhao, Xiangwei, McClelland, John F., Lu, Meng, 2016. Nanoscale 8 (46), 19204–19210.